De novo design of lipopeptide-based fusion inhibitor as potential broad-spectrum antiviral agent

Avijit Sardar[1], Sucharita Bhowmick[2], Mithila Kamble[2], Bibhas Hazra[1], Nikesh Dewangan[1], Amirul I. Mallick*[2], and Pradip K. Tarafdar*[1]

[1]Department of Chemical Sciences, [2]Department of Biological Sciences, Indian Institute of Science Education and Research Kolkata, Mohanpur-741246, India

---

*Corresponding authors:

Dr. Pradip Kumar Tarafdar
Department of Chemical Sciences
Indian Institute of Science Education and Research Kolkata
Mohanpur-741 246, India
E-mail: tarafdar@iiserkol.ac.in
ORCID iD: 0000-0002-1059-950X.

Dr. Amirul I. Mallick
Department of Biological Sciences
Indian Institute of Science Education and Research Kolkata
Mohanpur-741 246, India
E-mail: amallick@iiserkol.ac.in

Abstract

The recent surge in emerging viral infections warrants the need to design broad-spectrum antivirals. We aimed to develop a lead molecule that targets the membrane to block fusion, an obligate step of enveloped virus infection. The approach is based on the Coronin-1 protein of *Mycobacterium*, which presumably inhibits the phagosome-lysosome fusion, and a unique Trp-Asp (WD) sequence is placed at the distorted β-meander motif. We have designed a WD-based branched lipopeptide that supports C=O·····HN hydrogen-bonding, the tryptophan-tryptophan π-π stacking, and the intermolecular H-bonding between $–COO^-$ and $–CO_2H$ groups. These cooperative interactions are expected to create a β-sheet-like supramolecular assembly at the membrane surface, which increases the interfacial order, and decreases the water penetration. Myr-D$(WD)_2$ was shown to block artificial membrane fusion completely. We demonstrated that the Myr-D$(WD)_2$ supramolecular organization can restrict the infection from H1N1, H9N2, murine coronavirus, and human coronavirus (HCoV-OC43). Together, the present study provided an evidence-based broad-spectrum antiviral potential of a designed small lipopeptide.

Main

Emerging infectious diseases of viral origin pose a serious risk to public health and the global economy.[1,2] The world has recently witnessed the devastating effects of a novel coronavirus (SARS-CoV-2) pandemic outbreak affecting ~ 600 million humans with ~ 6.5 million deaths to date.[3] While global efforts to control SARS-CoV-2 infection are underway, only a few vaccines are available, with limited cross-protective ability.[4–6] The emergence of newer variants of SARS-CoV-2 invariably questions their long-lasting effects. Apart from the coronavirus infection, in recent times, Monkeypox has spread to several countries resulting in more than 35000 cases worldwide.[7] Seasonal influenza infection also remains a long-standing problem; frequent outbreaks of avian influenza and swine influenza virus have forced us to live under the unpredictable threat of pandemic outbreaks.[8,9] Dengue, West Nile, HIV, Hepatitis virus are also imminent threats to human health; however, has lower transmissibility. Nevertheless, new viruses present in the reservoir (estimated as half a million) may exhibit even a greater threat to human health in the near future.[10,11] Considering the impending risks associated with the emergence of viral infections, the development of effective broad-spectrum antiviral agents is the need of the hour.[12] The broad-spectrum antivirals presumably act on multiple viruses by targeting common but essential features of their life cycle. Notably, a vast majority of the viral pathogens such as HIV, Influenza, smallpox, flaviviruses, coronaviruses, etc., are membrane-enveloped viruses.[13] Host cell entry through 'membrane fusion' is the key early step for these viruses to replicate. During the membrane fusion, the viral lipid bilayer merges with the mammalian cell or subcellular membrane and the genetic material is released to the cytoplasm.[14] To perform this, viruses utilize specific fusion proteins that catalyze membrane fusion. A growing number of studies showed that the membrane fusion inhibitors that target specific viral fusion proteins can effectively tackle virus infection.[15–19] However, given the high rate of the mutability of the viruses, the effectiveness of such fusion inhibitors is limited and does not address the need for a broad-spectrum application. Therefore, instead of targeting the fusion protein, aiming at the intrinsic biophysical properties of viral or host cell membranes may be useful in tackling the infection caused by the enveloped viruses. To achieve this, RAFIs were developed, relying on their ability to promote positive curvature and thus, inhibit fusion and infection of several enveloped viruses.[20,21] In previous work, we exploited the *Mycobacterium*'s ability to evade phagosome-lysosome fusion and showed its translational potential by designing a small lipo-dipeptide (Myr-WD) fusion inhibitor.[22] *Mycobacterium* recruits Coronin-1, a member of WD40 domain protein, at the phagosomal membrane that

appears to play a crucial role in inhibiting the fusion of phagosome and lysosome.[23] The structure of Coronin-1 is unique from other WD40 proteins and the tryptophan-aspartic acid (WD) moiety is exposed at the edge of the distorted β-meander motif (**Figure 1**).[22] To develop a better membrane fusion inhibitor, we have customized the design of Myr-WD. A spacer to support branching was introduced. Aspartic acid backbone was chosen and it was acylated with a long chain fatty acid at *N*-terminus for anchoring to the membrane. Two WD units were attached to the two -CO_2H groups of the backbone aspartic acid (Myr-D$(WD)_2$). The design is expected to have several advantages, such as 1) in a membrane surface, lipopeptides may come closer and the –C=O·····HN– H-bonding between two molecules may be facilitated; 2) the tryptophan-tryptophan π-π stacking may be supported in the membrane interface; 3) the terminal –CO_2H group of two molecules may support the intermolecular H-bonding interactions between –COO^- and –CO_2H group; 4) the branching will facilitate these interactions from both sides that may lead to supramolecular assembly/cluster formation at the membrane surface; 5) these cooperative interactions may lead to a β-sheet-like structure (Coronin-1 WD are placed at the β-sheet region, **Figure 1**) from a simple lipopeptide. Extensive biophysical studies were employed to investigate the structure, membrane fusion inhibition, and membrane interfacial organization of Myr-D$(WD)_2$ and control peptides. We found that the dendrimer-type lipopeptide (Myr-D$(WD)_2$) completely blocks artificial membrane fusion, whereas the control peptides were not that efficient. The membrane fusion inhibition potential was utilized to tackle the infection of two Type A influenza viruses (H1N1, H9N2), murine coronavirus (RSA69), and human coronavirus (HCoV-OC43). Our studies strongly advocate the broad-spectrum antiviral potential of Myr-D$(WD)_2$.

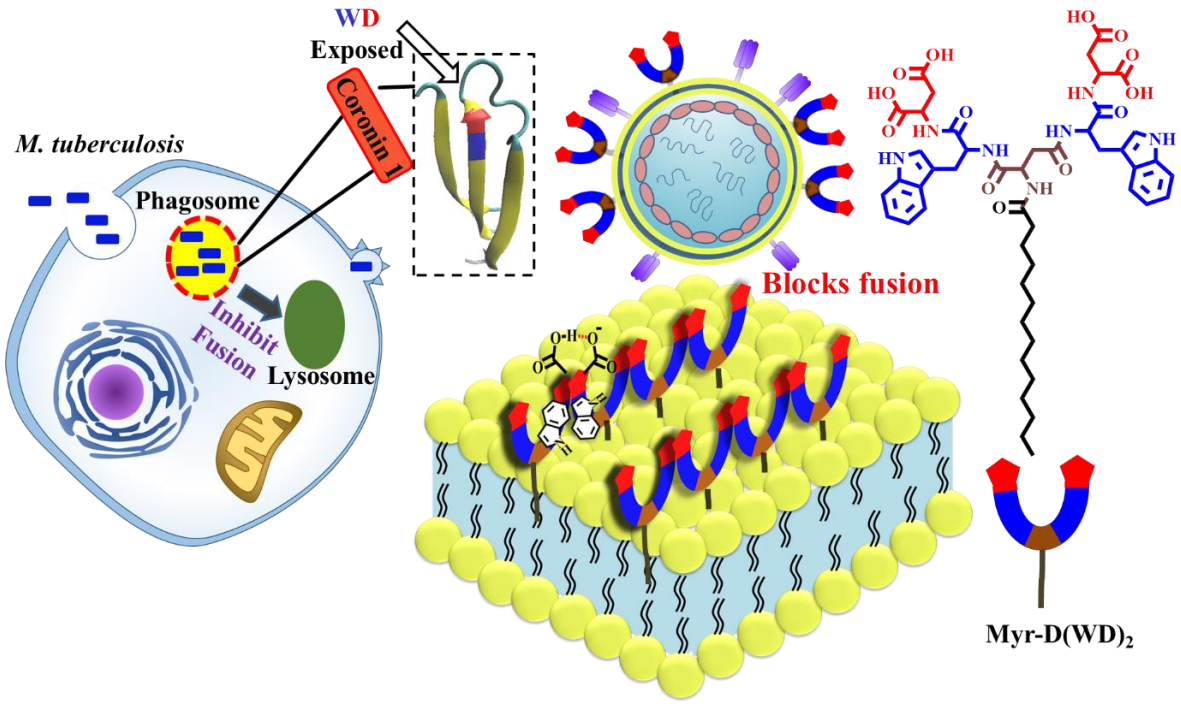

Figure 1: Phagosomal (*Mycobacterium tuberculosis*-infected) coat protein Coronin-1 inhibits the fusion with the lysosome. Coronin-1 structure shows Trp-Asp sequence (WD) are exposed and reside at the edge of the distorted β-meander motif (red: Asp, blue: Trp). A lipidated branched WD-based peptide (Myr-D(WD)$_2$) may self-assemble on the surface via π-π staking and COO^- ·····HOOC hydrogen bonding interactions. The self-assembled network stabilizes the membrane interface and inhibits the fusion between the host membrane and the enveloped viruses.

Results and discussion

Myr-D(WD)$_2$ was synthesized by standard solution phase protection-deprotection chemistry. We performed circular dichroism (CD) studies with the Myr-D(WD)$_2$ and found that it does not exhibit any secondary structure **(Figure 2A)**. Next, the peptide was incorporated into ~ 60 nm vesicles (DOPC/DOPE/Chol; 55/25/20) at a 25: 1 lipid to peptide ratio, and the CD was recorded. We found a negative peak at ~ 216 nm and a positive peak at ~ 200 nm, suggesting that the peptide with no secondary structure in solution, may adopt a β-sheet structure[24] in the presence of membrane **(Figure 2A)**. However, since the signal intensity was low (it is a pentapeptide), CD studies may not confirm the presence of a perfect β-sheet and thus, we refer it as a β-sheet-like structure. FT-IR studies (see the sample preparation in supporting information) of the lyophilized peptide exhibit a peak at ~ 1630 cm^{-1},[24,25] suggesting the possible presence of β-sheet-like structure **(Figure 2B)**. The formation of β-sheet-like structure

of a simple lipopeptide (Myr-D(WD)$_2$) in a membrane surface is remarkable. The control peptide (Myr-WD) with no branching (**Figure 3A**) does not adopt any secondary structure in the membrane as well as in the solution (**Figure S12**). It is possible that the β-sheet-like structure of Myr-D(WD)$_2$ may be stabilized by the Trp-Trp π-π stacking in the membrane. Next, the microenvironment of Trp was monitored by fluorescence spectroscopy. The fluorescence emission maxima of Myr-D(WD)$_2$ was ~ 362 nm in buffer (pH 5.5) and was blue-shifted to ~ 350 nm in the presence of DOPC/DOPE/Chol membrane **(Figure S11)**. The ~ 12 nm blue shift suggests that Trps of Myr-D(WD)$_2$ are embedded in the membrane interface.[26,27] Quenching studies with acrylamide and iodide and the Stern-Volmer quenching constants suggest that acrylamide was a better quencher than iodide (**Figure 2C**). This supports that the Trp is embedded in the membrane interface. Next, fluorescence anisotropy of Trp was measured at different peptide concentrations to evaluate the possibility of Trp-Trp interaction in the membrane (**Figure 2D**). The fluorescence anisotropy decreased with increasing the peptide concentration in membranes and the change was much sharper in pH 5.5 buffer as compared to that in pH 8.0 buffer. The decrease in fluorescence anisotropy likely is due to Homo-FRET, where the transfer of energy from one dipole to another leads to the depolarization of the emitted light.[28–30] The Homo-FRET between tryptophans suggests the possibility of π-π stacking between the Myr-D(WD)$_2$ molecules to stabilize the secondary structure. Since the Homo-FRET efficiency decreases at pH 8.0, it is possible that protonation and deprotonation equilibrium may also play an important role in the supramolecular interaction. At pH 5.5 the terminal –CO_2H of the aspartic acid will exist as protonated (–CO_2H) and deprotonated (–COO^-) form. The membrane interface may further perturb the pK_a,[31] and facilitate the localization of peptides to establish possible –COO^-·····HOOC– interactions. These interactions, which were proposed in prebiotic fatty acid vesicles,[32,33] might stabilize the Trp-Trp interactions in our system. We believe that these interactions (Trp-Trp, –COO^-·····HOOC–, and –C=O·····HN– H-bonding) might localize the peptide in the membrane and the branched design may lead to a supramolecular cluster formation (**Figure 1**). Next, NMR studies were performed in DOPC/DHPC, and DOPC/Chaps bicelles.[34] We compared the ^{1}H-NMR spectra of the Myr-D(WD)$_2$ peptide and Myr-WD (no branching, control peptide) in bicelles. The assignment of the hydrogens to the particular carbon (delta, epsilon, zeta, or eta) was confirmed by HSQC experiments in bicelles (**Figure S9**). The NMR peak corresponds to delta and epsilon hydrogen of tryptophan was broadened in Myr-D(WD)$_2$ as compared to Myr-WD **(Figure 2E and 2F)**. This suggests that the tryptophan environments in Myr-WD and Myr-D(WD)$_2$ are different. A new peak at the upfield region (0.05 ppm shift) appeared for the delta hydrogen of

Myr-D(WD)$_2$ in bicelles **(Figure 2E)**. The new peak and the broadening were absent when Myr-D(WD)$_2$ NMR was recorded in methanol. This suggests that the tryptophans of Myr-D(WD)$_2$ likely interact differently in bicelles. Next, we compared the NMR peaks of the delta, epsilon, eta, or zeta-1 hydrogens (ppm) position in bicelles and in methanol. We found that the epsilon, zeta-1, and eta proton shifted upfield in bicelles **(Figure 2E).** Since the protons of the tryptophan ring were shielded in bicelles, we suggest the possibility of Trp-Trp π-π stacking in a model membrane.[35,36] The Trp-Trp stacking interaction, and the H-bonding interactions between –C=O·····HN–, and –COO$^-$····HOOC– may stabilize the intermolecular interactions between Myr-D(WD)$_2$ in the membrane. The branch design with an Asp backbone will support these intermolecular interactions from both sides, which may lead to a supramolecular assembly/cluster formation in the membrane surface (**Figure 1**). The present model thus supports the CD data of Myr-D(WD)$_2$ which infers the possibility of β-sheet-like structures from a simple lipopeptide.

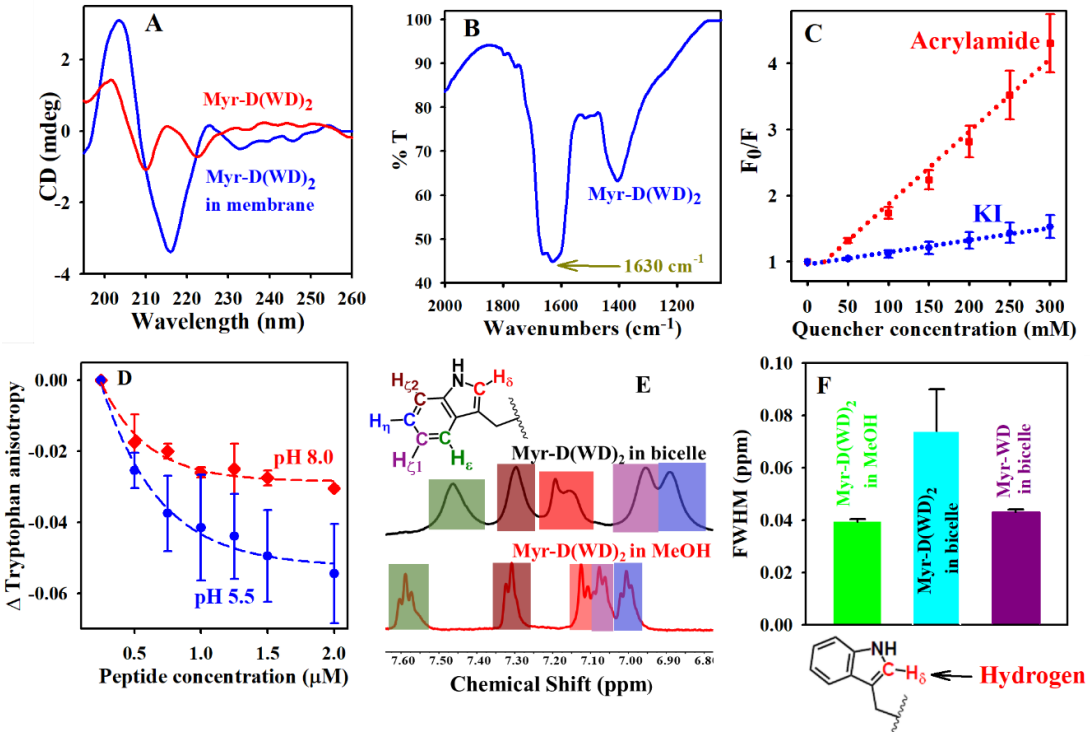

Figure 2. (A) CD spectra of Myr-D(WD)$_2$ in DOPC/DOPE/Chol (55/25/20) membranes at pH 5.5. (B) IR spectrum of Myr-D(WD)$_2$ exhibits a major peak at ~ 1630 cm^{-1}. (C) Acrylamide quenches the membrane-bound Myr-D(WD)$_2$ more than KI. (D) Homo-FRET of Myr-D(WD)$_2$ peptide at pH 5.5 (blue, ●), and pH 8.0 (red, ●) to measure Trp-Trp interaction. (E) ^{1}H-NMR spectra of Myr-D(WD)$_2$ in bicelle and MeOH. The NMR peak positions of the aromatic protons

were shifted. (F) Full-width half maxima of the delta hydrogen of Myr-D(WD)$_2$ in MeOH and bicelles, Myr-WD in bicelle.

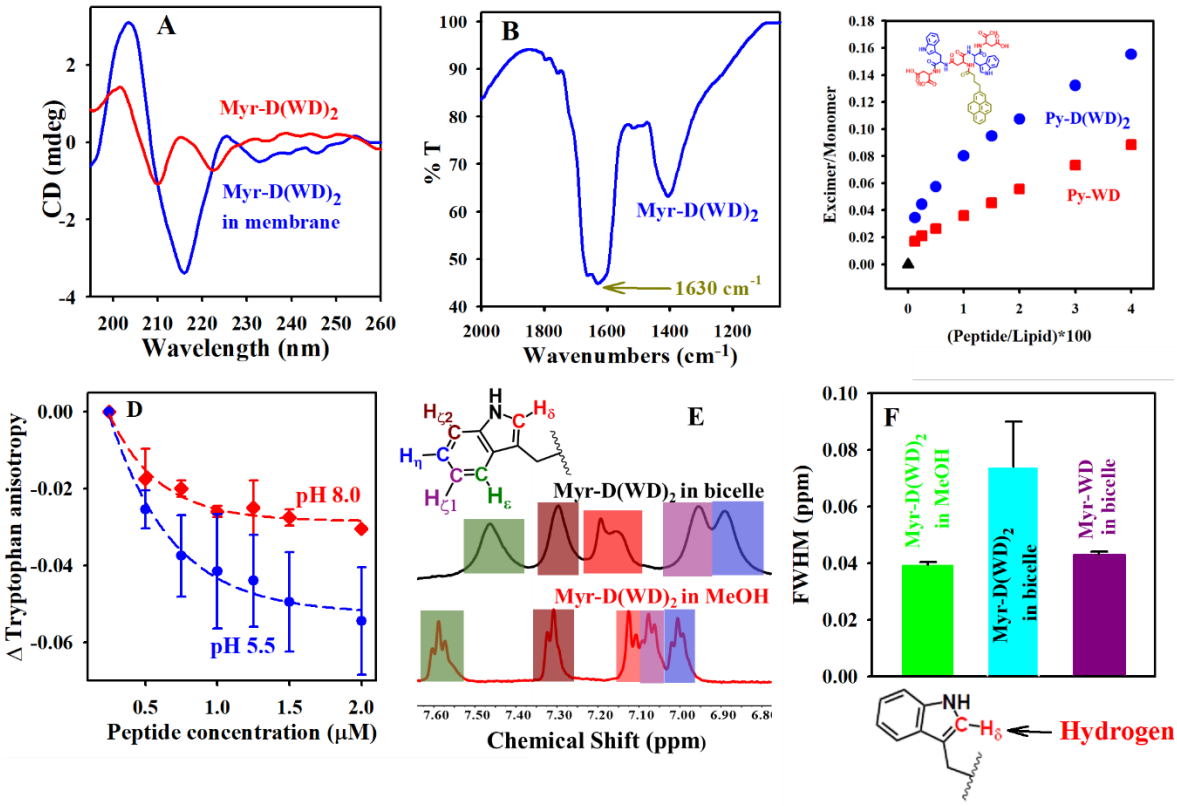

To check how the new design affects membrane fusion, FRET-based membrane fusion assays were carried out. Approximately 60 nm vesicles composed of DOPC/DOPE/Chol (55/25/20) vesicles and fluorophore-labeled vesicles DOPC/DOPE/Chol/NBD-PE/Rh-PE (55/22/20/1.5/1.5) vesicles were incubated at pH 5.5 MES buffer. The fusion was triggered by 6% (w/v) polyethylene glycol, and the kinetics was monitored by detecting the FRET dilution. The control vesicles exhibit ~ 25% fusion. We incorporated 2.0 μM Myr-D(WD)$_2$ in the vesicles and found that it completely arrested the fusion (lipid to peptide ratio of 100: 1). **(Figure 3A)**. It may be noted that our earlier design, Myr-WD at a similar lipid to peptide ratio inhibited the fusion but could not block the fusion **(Figure 3A)**.[22] Next, to test the role of tryptophan and aspartic acid, we synthesized a series of control peptides: Myr-D(D)$_2$ (without tryptophan), Myr-D(W)$_2$ (without Asp), Myr-D(WDMe)$_2$ (terminal -CO$_2$H protected with methyl ester), Myr-D(WG)$_2$ (Asp replaced by Gly), Myr-WWD (no branching). Among them, Myr-D(D)$_2$ with no Trp was found to slightly inhibit the fusion (from 25% to 23%), suggesting that tryptophan plays an important role to inhibit fusion. Next, we tested the efficacy of Myr-D(W)$_2$ with no terminal Asp at similar lipid to peptide ratio. Interestingly, the peptide inhibited the fusion but couldn't block the fusion. This suggests that the terminal Asp might also play an

important role. Next, the peptide Myr-WWD with two tryptophans was synthesized to test the role of branching (aspartic acid spacer). We found that although the extent of inhibition is similar in Myr-WWD and Myr-D$(W)_2$, the rate of fusion in Myr-WWD is higher than Myr-D$(W)_2$ (**Figure S10**). Therefore, despite having a terminal Asp, the Myr-WWD is less potent than Myr-D$(W)_2$, suggesting the importance of branched design. The binding affinity of the peptides to the membrane was measured by monitoring the tryptophan fluorescence intensity at various membrane concentrations. The K_d of Myr-D$(W)_2$, Myr-D$(WD)_2$, and Myr-WD were 34 ± 2 μM, 40 ± 4 μM, and 48 ± 3 μM[22]. WD peptide with no myristoyl chain neither binds the membrane nor inhibits the fusion. It suggests that the binding of the peptide (via lipid linker) to the membrane is essential to inhibit fusion. Finally, we compared the fusion inhibition ability of Myr-D$(WD)_2$ with Myr-D$(WG)_2$ and Myr-D$(WDMe)_2$. We found that Myr-D$(WD)_2$ with terminal Asp was a much superior inhibitor **(Figure 3D)**. It may be recalled that the Coronin-1 protein has exposed Trp-Asp placed at the distorted β-meander motif. We note that our present design, which contains Trp and Asp, adopts a β-sheet-like conformation in the membrane and is most effective in arresting fusion. Now the question rises, is there any correlation between the β-sheet-like structure and membrane fusion? Control peptides that could not completely block the fusion also do not adopt a β-sheet-like structure in the membrane, rather, a random structure was observed (**Figure S12**). We suggest that β-sheet-like supramolecular association of the peptide might stabilize the membrane interface to arrest fusion. We conclude that the architectural orientation of the molecule and the myristoyl lipid linker, aspartate spacer (branch), tryptophan, and aspartic acid worked in tandem to exhibit the superior fusion inhibition ability of Myr-D$(WD)_2$.

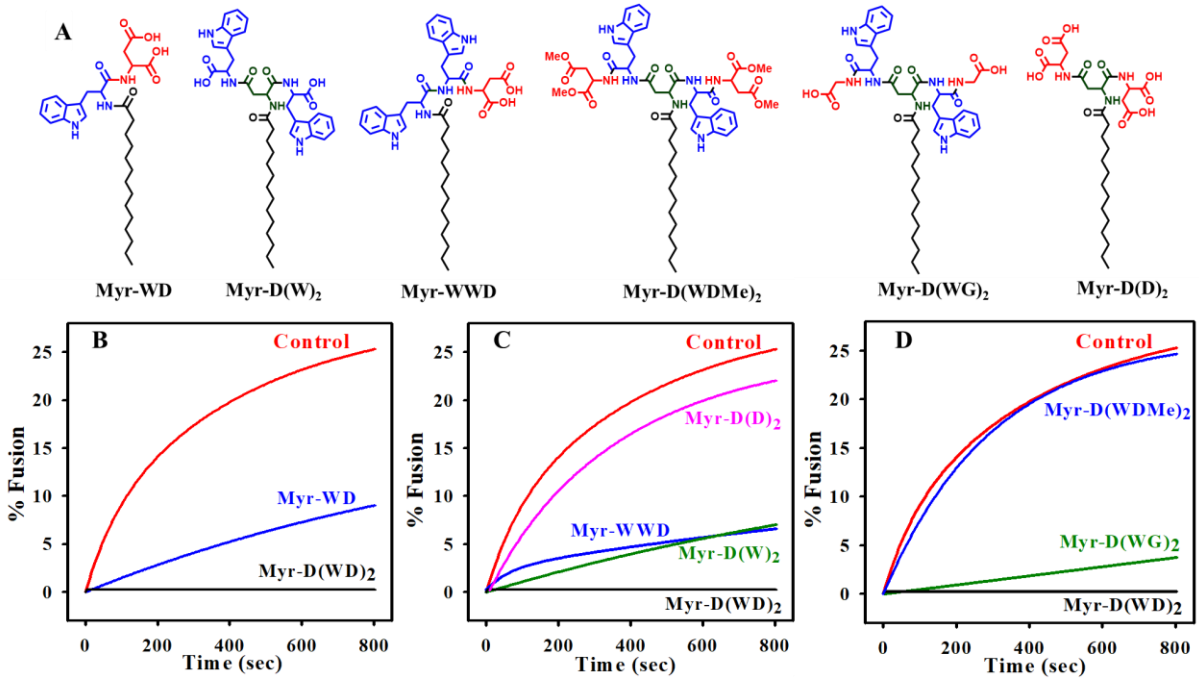

Figure 3. (A) Structures of the control lipidated peptides. (B) Comparison of earlier design (Myr-WD) and the new design (Myr-D(WD)$_2$). (C) the role of aspartate backbone as a spacer and the role of tryptophan, and (D) the role of terminal aspartic acid of the lipo-peptide. The fusion kinetics were carried out in 20 mM MES, 50 mM NaCl, pH 5.5 at a total lipid concentration of 200 μM, and the peptide to lipid ratio were kept at 1: 100.

To understand the fusion kinetics, concentration-dependent studies were performed. We found that the initial rate and extent of fusion decrease with the increase in peptide concentration (**Figure 4A and S10B**). Next, TMA-DPH anisotropy at the membrane interface was measured in the presence of peptides to understand how these peptides affect the membrane interfacial region. The TMA-DPH anisotropy increased linearly with the increase of Myr-D(WD)$_2$ peptide concentration **(Figure 4B)**. Our earlier peptide (Myr-WD) also increased the TMA-DPH anisotropy but in a hyperbolic fashion.[22] These studies confirm that the membrane organization of Myr-D(WD)$_2$ and Myr-WD is different. The control peptide where the terminal -CO_2H groups were protected (Myr-D(WDMe)$_2$) did not increase the anisotropy. The increase in TMA-DPH anisotropy suggests the ordering or stabilization of the interface by Myr-D(WD)$_2$. This may retard the lipid protrusion, required for hemifusion intermediate formation.[37,38]

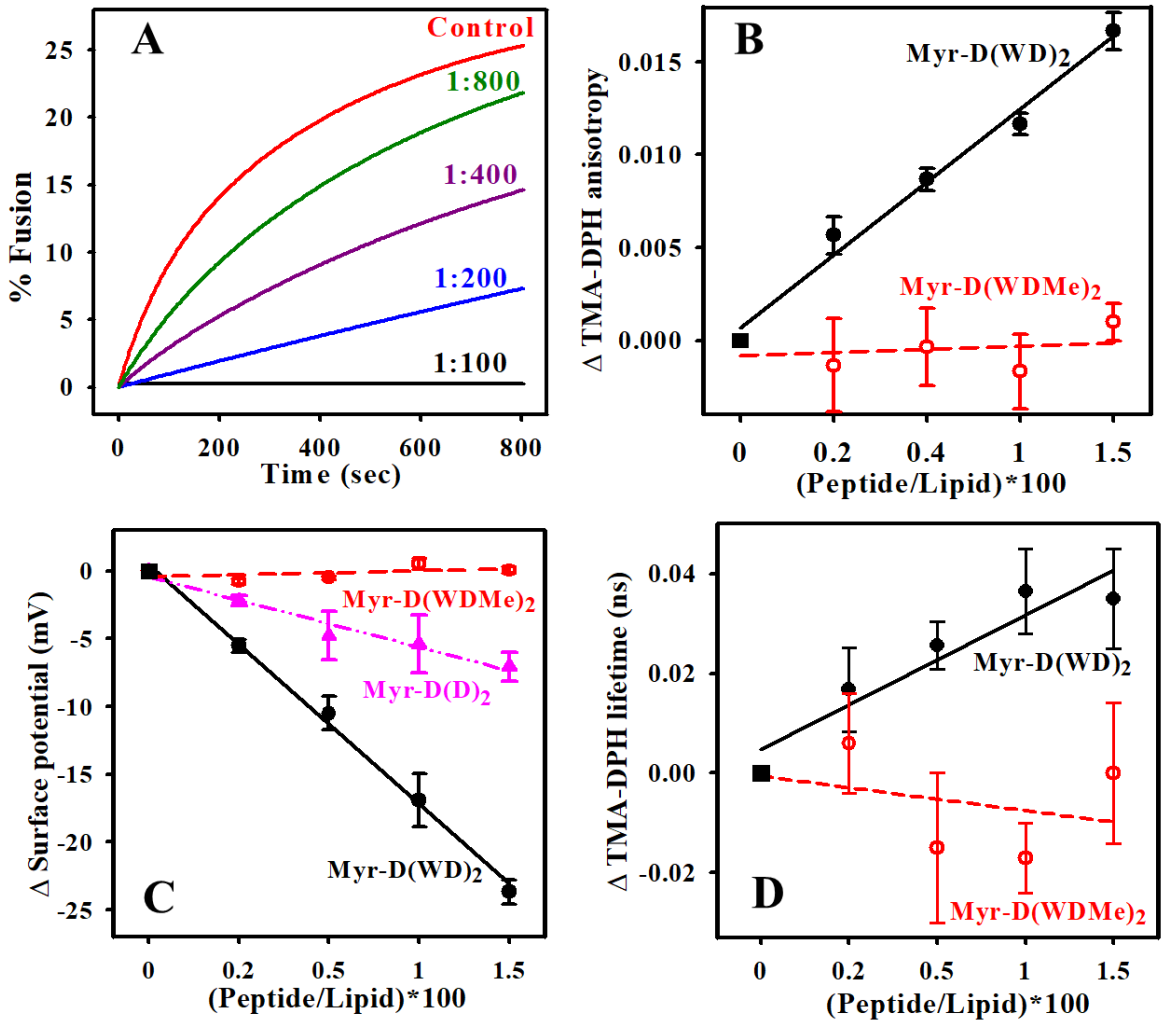

Figure 4. Mechanistic studies on the inhibition of fusion. (A) Myr-D(WD)$_2$ inhibits the fusion of DOPC/DOPE/Chol (55/25/20)vesicles in a concentration-dependent manner, (B) change in the fluorescence anisotropy of TMA-DPH in DOPC/DOPE/Chol (55/25/20) membranes with increasing concentration of Myr-D(WD)$_2$ (black, ●) and Myr-D(WDMe)$_2$ (red, ●), (C) change in the zeta potential (mV) with increasing concentration of Myr-D(WD)$_2$, Myr-D(D)$_2$ (pink, ●) and Myr-D(WDMe)$_2$ (red, ●). (D) change in the average fluorescence lifetime (ns) of TMA-DPH in the presence of peptides.

Next, we measured the zeta potential of the membrane at various peptide concentrations. We observed that Myr-D(WDMe)$_2$ does not decrease the zeta potential, whereas the incorporation of Myr-D(WD)$_2$ in the membrane linearly decreases the zeta potential **(Figure 4C)**. Another control peptide with the terminal aspartic acids (Myr-D(D)$_2$) was investigated to understand whether the WD sequence is special! We found that Myr-D(D)$_2$ decreases the zeta potential, but the extent of the decrease in the zeta potential of Myr-D(WD)$_2$ is more prominent (four

times more) than Myr-D(D)$_2$. The negative zeta potential of Myr-D(WD)$_2$ may induce charge-charge repulsion to retard hemifusion intermediate formation.[39]

Further, we investigated the TMA-DPH lifetime at various peptide to lipid ratios to understand the extent of water penetration in the interfacial region **(Figure 4D)**. The average TMA-DPH lifetime increased linearly with Myr-D(WD)$_2$ concentration in the membrane. Therefore, the fusion inhibitory peptide Myr-D(WD)$_2$ might decrease the water penetration at the interface.[40] The average lifetime did not increase with the Myr-D(WDMe)$_2$ peptide supports the above argument. During hemifusion (a necessary step for fusion), the lipid and water may mix to support protrusion.[37,38] Therefore, reduction of water penetration in the membrane by Myr-D(WD)$_2$ is another key feature of fusion inhibition. We conclude that the branched design (Myr-D(WD)$_2$) is a unique lipopeptide that effectively inhibits the fusion via the modulation of several physicochemical properties: binding to the membrane, Trp-Trp interaction, adopting a β-sheet-like structure, the increase in the interfacial order, and the decrease in the zeta potential and the water penetration.

Since the Myr-D(WD)$_2$ peptide was an excellent membrane fusion inhibitor, we anticipated that it could tackle viral infection by inhibiting the viral membrane fusion. The antiviral activity of the lipopeptide was tested in MDCK cells against two Type A influenza viruses, A/PR/8/34 (H1N1) and A/turkey/Wisconsin/1/1966 (H9N2). The cell survivability experiments suggest that Myr-D(WD)$_2$ offer ~ 60% protection at ~3.0 μM concentration. We note that Myr-D(WD)$_2$ is ~ twice more effective than Myr-WD at 3 μM concentration, which is consistent with the better fusion inhibitory effect of the molecule **(Figure 3B)**. At a low concentration of ~190 nM, the peptide offers nearly 40% protection (**Figure 5A**). Similarly, in the case of H9N2 virus infection, the protective efficacy was ~ 60-50% when the Myr-D(WD)$_2$ was used at ~3.0 μM to 90 nM concentration **(Figure S15)**. Further, a significant reduction in viral plaque formation for both subtypes of the influenza viruses was also observed with the treatment of ~ 3.0 μM and 1.5 μM of Myr-D(WD)$_2$. This observation was further substantiated by the difference in cell cytopathic effects (CPEs) **(Figure 5C, S15**). Next, we performed indirect immunofluorescence assay[41] using FITC labeled anti-NP antibody. The results show a significantly low background with minor antibody immunoreactivity against the viral NP protein in the infected cells treated with 3.0 μM Myr-D(WD)$_2$. This suggests an effective reduction in the accumulation of viral NP **(Figure 5D, S15)**. All these experiments support the antiviral activity of Myr-D(WD)$_2$ against H1N1 and H9N2 infections.

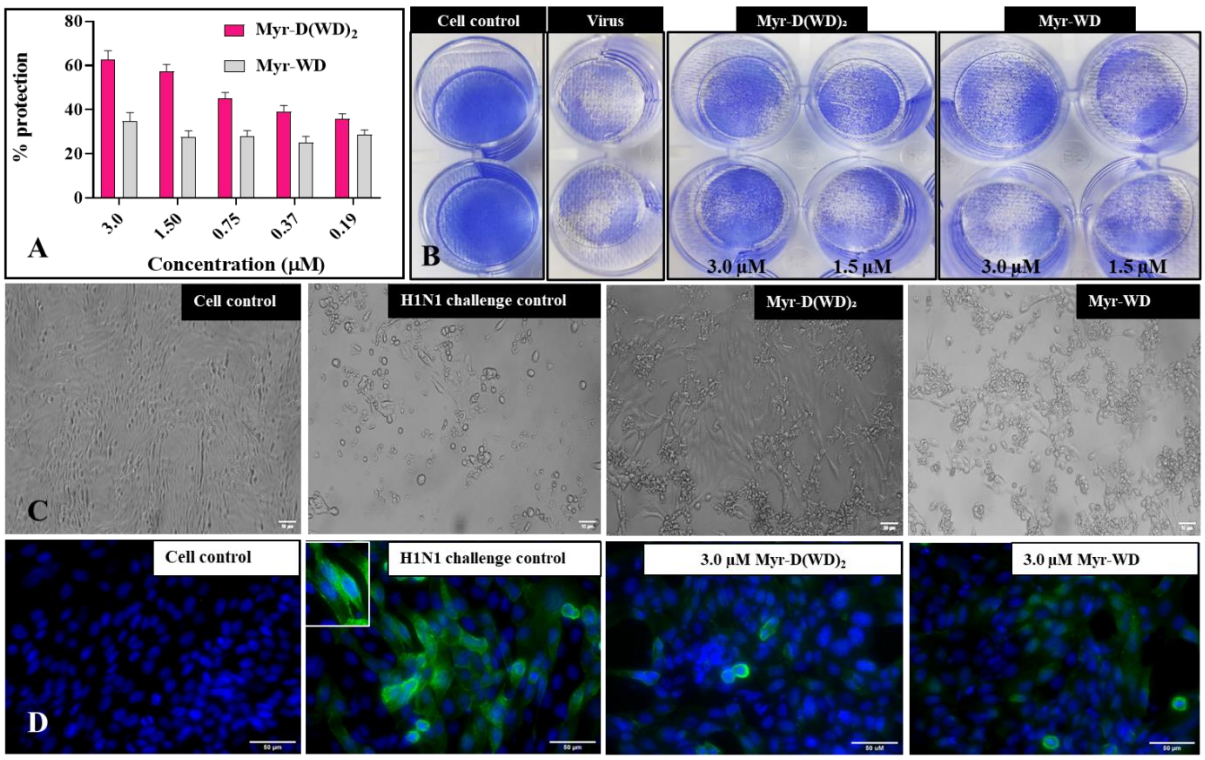

Figure 5. Determination of the antiviral activity of Myr-D(WD)$_2$ on influenza A/PR/8/1934 (H1N1) virus infection in MDCK cells. (A) Viability of MDCK cells in a dose-dependent manner was assessed using a standard MTT-based assay after H1N1 virus infection and drug treatment for ~ 30-36 h. (B) Inhibitory effect of the compound on plaque formation after 48 h indicates the reduced H1N1 plaque formation. Myr-D(WD)$_2$ protects more as compared to Myr-WD. (C) Images of the CPEs were captured by an inverted light microscope (Nikon, Japan) at 20X magnification. (D) Myr-D(WD)$_2$ reduces viral NP protein accumulation in the cytoplasm of viral-infected cells as measured by the indirect immunofluorescence assay.

The antiviral effect of Myr-D(WD)$_2$ was further explored in the L2 cells using RSA59, an isogenic recombinant strain of mouse hepatitis virus, belonging to the β-coronavirus group (murine coronavirus).[42] Plaque assay in L2 cells cotreated with virus and inhibitor peptide (50 µM) suggests the potent antiviral effect of Myr-D(WD)$_2$ (**Figure 6A**). The antiviral effect of peptides on the fusogenicity of RSA59 (expresses enhanced green fluorescent protein) was assessed by analyzing the syncytial formation on cotreatment with the virus (at 0.5 MOI) and the lipopeptide inhibitor. Myr-D(WD)$_2$ significantly reduced the syncytia formation (**Figure 6B**). We further tested the efficacy of the Myr-D(WD)$_2$ against human coronavirus infection (HCoV-OC43). The designed compound shows ~ 100% protection at 25.0 µM concentration and ~ 40% protection at the nanomolar concentration (780 nM). These data were further

validated by a significant reduction in cell cytopathic effects (CPEs) of Vero cells infected with HCoV-OC43 **(Figure 6C and D)**.

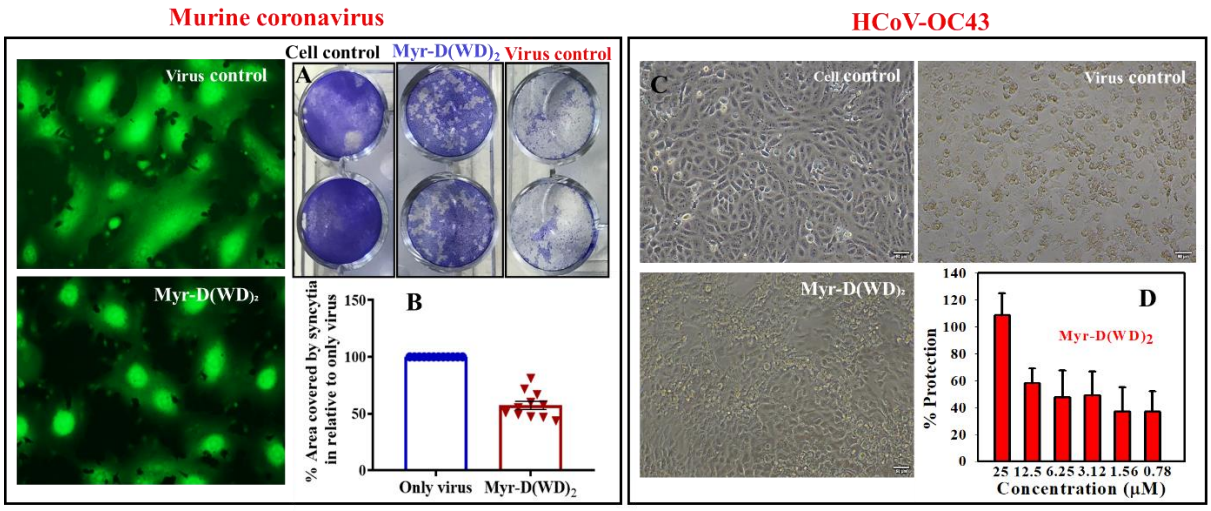

Figure 6. Myr-D(WD)$_2$ protects from the murine coronavirus (RSA59) and human coronavirus (HCoV-OC43) infection. (A) Myr-D(WD)$_2$ reduced viral plaque formation in L2 cells. (B) Myr-D(WD)$_2$ significantly reduced syncytia formation. Left panel: Fluorescence images of syncytia formation. (C) Images of the cell cytopathic effects (HCoV-OC43 infection) were captured by an inverted light microscope at 20X magnification. (D) The viability of Vero cells was assessed using a range of concentrations and performing a standard MTT assay. The drug treatment was given after 6 days post-infection with HCoV-OC43.

Membrane-enveloped viruses have caused several episodes of endemics and pandemics in modern times.[43] Therefore, the development of broad-spectrum antivirals that target a wide range of enveloped viruses is essential for controlling the present or any future pandemics. The broad-spectrum antivirals might inhibit the enveloped virus membrane fusion to exhibit efficacy. Most reports to design a fusion inhibitor[44] are based on targeting the receptor binding domain or fusion domain with the peptides,[15,18,45–50] small molecules,[51,52] lectins,[53–55] antibodies,[56] etc. However, the scope for targeting the fusion machinery of a specific virus is limited to that particular infection and hence can not be used against multiple viruses. Therefore, membrane-active therapeutics that passively interfere with membrane fusion[21,22] or membranolytic compounds that attack the viral envelope[15,43] can act as broad-spectrum antivirals. Coronin-1, a *Mycobacterium* protein apparently inhibits phagosome-lysosome fusion has a unique feature where the Trp-Asp sequence resides at the distorted β-meander motif.[22] Inspired by Coronin-1, WD-based peptides with the β-sheet structure were designed and synthesized. We found that a branched design (Myr-D(WD)$_2$) may facilitate H-bonding

interactions, the Trp-Trp π-π stacking interactions from both sides that eventually lead to a supramolecular assembly in the membrane (**Figure 1**). The Myr-WD (no branch) and control peptides, which could not completely block the membrane fusion, do not adopt a β-sheet structure and do not linearly modulate the interfacial physical properties.[22] We have shown that the effective fusion inhibitor (Myr-D$(WD)_2$) is also more potent in tackling infections from four different viruses at micromolar to nanomolar concentrations.

Conclusions

We have exploited the survival strategy of the *Mycobacterium* by Coronin-1 coat protein to design a WD-based branched lipopeptide (Myr-D$(WD)_2$) that assembles in the membrane and adopts a β-sheet-like structure. While the control peptides could not arrest the fusion, the branched design completely inhibits membrane fusion. The spectacular membrane fusion inhibitory effect of the lipopeptide was utilized to protect the cells from four different viruses: Type A influenza virus H1N1, H9N2, murine coronavirus (RSA59), and human coronavirus (HCoV-OC43). Our simple lipopeptide could be a potential broad-spectrum antiviral compound to tackle a variety of deadly viruses. Finally, the concept of membrane-assisted supramolecular assembly and β-sheet-like organization of a membrane-active small molecule and its passive role in fusion inhibition by ordering the membrane interface is novel. A similar concept may be applied to alter the membrane interfacial property to induce allostery in membrane proteins of pharmaceutical interest.

Online Methods

Materials and methods, Supplementary text, Figs. S1–16, copies of NMR spectra, and references are compiled in the supplementary file.

References

1. Jones, K. E. *et al.* Global trends in emerging infectious diseases. *Nature* **451**, 990 (2008).

2. Morens, D. M. & Fauci, A. S. Emerging Infectious Diseases: Threats to Human Health and Global Stability. *PLoS Pathog* **9**, e1003467 (2013).

3. WHO Coronavirus (COVID-19) Dashboard | WHO Coronavirus (COVID-19) Dashboard With Vaccination Data. https://covid19.who.int/.

4. Dacon, C. *et al.* Broadly neutralizing antibodies target the coronavirus fusion peptide. *Science* **377**, 728–735 (2022).

5. Planas, D. *et al.* Considerable escape of SARS-CoV-2 Omicron to antibody neutralization. *Nature* **602**, 671–675 (2022).

6. Sievers, B. L. *et al.* Antibodies elicited by SARS-CoV-2 infection or mRNA vaccines have reduced neutralizing activity against Beta and Omicron pseudoviruses. *Sci Transl Med* **14**, eabn7842 (2022).

7. 2022 Monkeypox Outbreak Global Map | Monkeypox | Poxvirus | CDC. https://www.cdc.gov/poxvirus/monkeypox/response/2022/world-map.html.

8. Butler, D. Swine flu goes global. *Nature* **458**, 1082–1083 (2009).

9. Yong, E. Influenza: Five questions on H5N1. *Nature* **486**, 456–458 (2012).

10. Caminade, C., McIntyre, K. M. & Jones, A. E. Impact of recent and future climate change on vector-borne diseases. *Annals of the New York Academy of Sciences* **1436**, 157-173 (2019).

11. Morse, S. S. *et al.* Prediction and prevention of the next pandemic zoonosis. *The Lancet* **380**, 1956–1965 (2012).

12. Vigant, F., Santos, N. C. & Lee, B. Broad-spectrum antivirals against viral fusion. *Nature Reviews Microbiology* **13,** 426–437 (2015).

13. Rey, F. A. & Lok, S. M. Common Features of Enveloped Viruses and Implications for Immunogen Design for Next-Generation Vaccines. *Cell* **172**, 1319–1334 (2018).

14. Plemper, R. K. Cell entry of enveloped viruses. *Current Opinion in Virology* **1**, 92–100 (2011).

15. Jackman, J. A. Antiviral peptide engineering for targeting membrane-enveloped viruses: Recent progress and future directions. *Biochimica et Biophysica Acta (BBA) - Biomembranes* **1864**, 183821 (2022).

16. Schütz, D. *et al.* Peptide and peptide-based inhibitors of SARS-CoV-2 entry. *Adv Drug Deliv Rev* **167**, 47–65 (2020).

17. Xia, S. *et al.* A pan-coronavirus fusion inhibitor targeting the HR1 domain of human coronavirus spike. *Sci Adv* **5**, eaav4580 (2019).

18. de Vries, R. D. *et al.* Intranasal fusion inhibitory lipopeptide prevents direct-contact SARS-CoV-2 transmission in ferrets. *Science* **371**, 1379–1382 (2021).

19. Zhu, Y., Yu, D., Yan, H., Chong, H. & He, Y. Design of Potent Membrane Fusion Inhibitors against SARS-CoV-2, an Emerging Coronavirus with High Fusogenic Activity. *J Virol* **94**, e00635-20 (2020).

20. Vigant, F., Jung, M. & Lee, B. Positive reinforcement for viruses. *Chemistry and Biology* **17**, 1049-1051 (2010).

21. st. Vincent, M. R. *et al.* Rigid amphipathic fusion inhibitors, small molecule antiviral compounds against enveloped viruses. *Proc Natl Acad Sci U S A* **107**, 17339–17344 (2010).

22. Sardar, A., Lahiri, A., Kamble, M., Mallick, A. I. & Tarafdar, P. K. Translation of Mycobacterium Survival Strategy to Develop a Lipo-peptide based Fusion Inhibitor. *Angewandte Chemie International Edition* **60**, 6101–6106 (2021).

23. Ferrari, G., Langen, H., Naito, M. & Pieters, J. A coat protein on phagosomes involved in the intracellular survival of mycobacteria. *Cell* **97**, 435–447 (1999).

24. Pashuck, E. T., Cui, H. & Stupp, S. I. Tuning Supramolecular Rigidity of Peptide Fibers through Molecular Structure. *J Am Chem Soc* **132**, 6041–6046 (2010).

25. Miki, T. *et al.* Intracellular artificial supramolecules based on de novo designed Y15 peptides. *Nature Communications* **12**, 1–11 (2021).

26. Vivian, J. T. & Callis, P. R. Mechanisms of Tryptophan Fluorescence Shifts in Proteins. *Biophys J* **80**, 2093–2109 (2001).

27. Tarafdar, P. K., Chakraborty, H., Bruno, M. J. & Lentz, B. R. Phosphatidylserine-Dependent Catalysis of Stalk and Pore Formation by Synaptobrevin JMR-TMD Peptide. *Biophys J* **109**, 1863–1872 (2015).

28. Meher, G., Bhattacharjya, S. & Chakraborty, H. Membrane Cholesterol Modulates Oligomeric Status and Peptide-Membrane Interaction of Severe Acute Respiratory Syndrome Coronavirus Fusion Peptide. *Journal of Physical Chemistry B* **123**, 10654–10662 (2019).

29. Chakraborty, H. & Chattopadhyay, A. Excitements and challenges in GPCR oligomerization: Molecular insight from FRET. *ACS Chem Neurosci* **6**, 199–206 (2015).

30. Ganguly, S., Clayton, A. H. A. & Chattopadhyay, A. Organization of higher-order oligomers of the serotonin$_1$(A) receptor explored utilizing homo-FRET in live cells. *Biophys J* **100**, 361–368 (2011).

31. Sardar, A. *et al.* A headgroup linker perturbs pKavia acyl chain migration: designing base-labile supramolecular assemblies. *Chemical Communications* **54**, 4282–4285 (2018).

32. Kundu, N., Mondal, D. & Sarkar, N. Dynamics of the vesicles composed of fatty acids and other amphiphile mixtures: unveiling the role of fatty acids as a model protocell membrane. *Biophys Rev* **12**, 1117 (2020).

33. Dejanović, B., Noethig-Laslo, V., Šentjurc, M. & Walde, P. On the surface properties of oleate micelles and oleic acid/oleate vesicles studied by spin labeling. *Chem Phys Lipids* **164**, 83–88 (2011).

34. Warschawski, D. E. *et al.* Choosing membrane mimetics for NMR structural studies of transmembrane proteins. *Biochimica et Biophysica Acta (BBA) - Biomembranes* **1808**, 1957–1974 (2011).

35. Shao, C., Grüne, M., Stolte, M. & Würthner, F. Perylene Bisimide Dimer Aggregates: Fundamental Insights into Self-Assembly by NMR and UV/Vis Spectroscopy. *Chemistry – A European Journal* **18**, 13665–13677 (2012).

36. Sao, S., Naskar, S., Mukhopadhyay, N., Das, M. & Chaudhuri, D. Assisted π-stacking: a strong synergy between weak interactions. *Chemical Communications* **54**, 12186–12189 (2018).

37. Kasson, P. M., Lindahl, E. & Pande, V. S. Water ordering at membrane interfaces controls fusion dynamics. *J Am Chem Soc* **133**, 3812–3815 (2011).

38. Chakraborty, H., Tarafdar, P. K., Klapper, D. G. & Lentz, B. R. Wild-type and mutant hemagglutinin fusion peptides alter bilayer structure as well as kinetics and activation thermodynamics of stalk and pore formation differently: Mechanistic implications. *Biophys J* **105**, 2495–2506 (2013).

39. Tarafdar, P. K., Chakraborty, H., Dennison, S. M. & Lentz, B. R. Phosphatidylserine inhibits and calcium promotes model membrane fusion. *Biophys J* **103**, 1880–1889 (2012).

40. Demchenko, A. P., Mély, Y., Duportail, G. & Klymchenko, A. S. Monitoring biophysical properties of lipid membranes by environment-sensitive fluorescent probes. *Biophysical Journal* vol. **96**, 3461–3470 (2009).

41. Lahiri, A., Bhowmick, S., Sharif, S. & Mallick, A. I. Pre-treatment with chicken IL-17A secreted by bioengineered LAB vector protects chicken embryo fibroblasts against Influenza Type A Virus (IAV) infection. *Mol Immunol* **140**, 106–119 (2021).

42. Sarkar, L., Putchala, R. K., Safiriyu, A. A. & Das Sarma, J. Azadirachta indica A. Juss Ameliorates Mouse Hepatitis Virus-Induced Neuroinflammatory Demyelination by Modulating Cell-to-Cell Fusion in an Experimental Animal Model of Multiple Sclerosis. *Front Cell Neurosci* **14**, 1-22 (2020).

43. Yoon, B. K., Jeon, W. Y., Sut, T. N., Cho, N. J. & Jackman, J. A. Stopping Membrane-Enveloped Viruses with Nanotechnology Strategies: Toward Antiviral Drug Development and Pandemic Preparedness. *ACS Nano* **15**, 125–148 (2021).

44. Xiu, S. *et al.* Inhibitors of SARS-CoV-2 Entry: Current and Future Opportunities. *J Med Chem* **63**, 12256–12274 (2020).

45. Dwyer, J. J. *et al.* Design of helical, oligomeric HIV-1 fusion inhibitor peptides with potent activity against enfuvirtide-resistant virus. *Proc Natl Acad Sci U S A* **104**, 12772–12777 (2007).

46. Pessi, A. *et al.* A General Strategy to Endow Natural Fusion-protein-Derived Peptides with Potent Antiviral Activity. *PLoS One* **7**, e36833 (2012).

47. Kadam, R. U. *et al.* Potent peptidic fusion inhibitors of influenza virus. *Science* **358**, 496–502 (2017).

48. van Dongen, M. J. P. *et al.* A small-molecule fusion inhibitor of influenza virus is orally active in mice. *Science* **363**, eaar6221 (2019).

49. Xia, S. *et al.* Inhibition of SARS-CoV-2 (previously 2019-nCoV) infection by a highly potent pan-coronavirus fusion inhibitor targeting its spike protein that harbors a high capacity to mediate membrane fusion. *Cell Research* **30**, 343–355 (2020).

50. Zhu, Y. *et al.* SARS-CoV-2-derived fusion inhibitor lipopeptides exhibit highly potent and broad-spectrum activity against divergent human coronaviruses. *Signal Transduction and Targeted Therapy* **6**, 1–3 (2021).

51. Bojadzic, D. *et al.* Small-Molecule Inhibitors of the Coronavirus Spike: ACE2 Protein-Protein Interaction as Blockers of Viral Attachment and Entry for SARS-CoV-2. *ACS Infect Dis* **7**, 1519–1534 (2021).

52. Li, Y. T. *et al.* Axial Chiral Binaphthoquinone and Perylenequinones from the Stromata of Hypocrella bambusae Are SARS-CoV-2 Entry Inhibitors. *J Nat Prod* **84**, 436–443 (2021).

53. Sarkar, A. *et al.* A novel plant lectin, NTL-125, interferes with SARS-CoV-2 interaction with hACE2. *Virus Res* **315**, 19768 (2022).

54. Liu, Y. M. *et al.* A Carbohydrate-Binding Protein from the Edible Lablab Beans Effectively Blocks the Infections of Influenza Viruses and SARS-CoV-2. *Cell Rep* **32**, 108016 (2020).

55. Keeffe, J. R. *et al.* Designed oligomers of cyanovirin-N show enhanced HIV neutralization. *Proc Natl Acad Sci U S A* **108**, 14079–14084 (2011).

56. Corti, D., Purcell, L. A., Snell, G. & Veesler, D. Tackling COVID-19 with neutralizing monoclonal antibodies. *Cell* **184**, 3086–3108 (2021).

Data availability

The data that support the findings of this study are available within the paper and its Supplementary Information.

Acknowledgments

We thank IISER Kolkata for its generous support (ARF). P.K.T. acknowledges support from DST-Inspire and the Science and Engineering Research Board (SERB). A.S., S.B., and M.K. thank UGC; B.H. and N.D. thank CSIR for their fellowship. We thank Prof. Jayasri Das Sarma and Dr. Manmeet Singh for murine coronavirus studies.

Funding

PKT sincerely thanks the Science and Engineering Research Board (SERB) Early Career Award (Grant No: ECR/2016/001935) and Core Research Grant (Grant No: CRG/2022/008554) for the financial support.

Contributions

A.S. and P.K.T. conceived and designed the project. A.S., B.H, and N.D. performed the synthetic experiments. A.S. and B.H. performed biophysical experiments. S.B. and M.K. performed cell experiments. A.S., S.B., M.K., A.I.M., and P.K.T. analyzed the data. A.S., A.I.M., and P.K.T. wrote the manuscript.

Competing interests

The authors declare no competing interests.